Drying kinetics and effective water diffusivities in olive stone and olive-tree pruning

Manuel Cuevas[a], María Lourdes Martínez-Cartas[a], Luis Pérez-Villarejo[a], Lucía Hernández[a], Juan Francisco García-Martín[b]*, Sebastián Sánchez[a]

[a]Department of Chemical, Environmental and Materials Engineering, University of Jaén, Campus 'Las Lagunillas', 23071 Jaén, Spain

[b]Department of Chemical Engineering, University of Seville, C/ Profesor García Gonzalez, 1, 41012 Seville, Spain

*Corresponding author. *E-mail address:* jfgarmar@us.es

Abstract

Drying kinetics of olive stone and olive-tree pruning, two important biomasses from olive culture, was experimentally assessed at six different temperatures (from 343 K to 393 K) and four sample thicknesses (from 15 to 50 mm). Analysis of the drying curves revealed that Page's model was suitable for predicting the drying characteristics of both solid biofuels. From this analysis, two new mathematical equations to describe the dependence of moisture ratio with temperature and drying time were also proposed. The values of effective water diffusivity, calculated at the falling rate period by using Fick's second law of diffusion, increased when increasing drying temperature and sample thickness. Diffusivities for olive-tree pruning ($3.41 \times 10^{-8} - 32.5 \times 10^{-8}$ m^2/s) were almost twice higher than those for olive stone ($1.87 \times 10^{-8} - 16.4 \times 10^{-8}$ m^2/s).

Keywords: olive stone; olive-tree pruning; drying; mathematical modelling; effective diffusivity.

1. Introduction

Developed countries are constantly striving to achieve a stable source of renewable energy to reduce their dependence on fossil fuels and fight against global warming. In the European Union, biomass is expected to contribute to around half of the renewable energy share in 2020 according to projections [1]. Therefore, the use of all available biomasses for energy production in a sustainable way should be taken into account.

Over 11 million ha olive trees are cultivated worldwide, mainly in the Mediterranean countries [2]. The olive culture plays a vital role in the economic and social development of these countries. Spain produces about 33% of the world's olive oil [3]. More than 350 million olives are grown all over Spain, most of them in the southern region of Andalusia where olive groves represent roughly 1.55×10^6 ha cultivated land [4].

The industrial processing of the olive fruit as well the management of olive orchard generates lignocellulosic by-products such as olive stone and olive-tree pruning, respectively. In olive oil mills, decanters of two exits separate a liquid stream (olive oil) and a solid stream (pomace) [5]. Fragmented olive stones are then separated from olive pomace by pitting machines. Around 0.6 t olive stones are estimated to be produced in the olive mills per hectare olive grove [2], resulting in a worldwide production of 6.6×10^6 t/year. Olive stone (OP) can be used for different applications (bioethanol [6], activated carbon [7], furfural production [8], natural antioxidants [9] ...) however the vast majority of olive stone production is used for thermal energy generation due to its high heating value and density, low ash, nitrogen and sulphur content, and uniform particle size [10]. On the other hand, pruning operation is essential to enhance the productivity of olive grove because it helps to remove unproductive branches thus enhancing air circulation and light penetration though the foliage to prevent microbial diseases. Given that one hectare of olive grove can annually produce on average 3 t of pruning [2,11], it can be estimated that the annual worldwide production of this biomass is around 3.3 × 10^7 t, which illustrates the great availability and potential of this biomass for energy production. However, in most cases olive-tree pruning (OP) is left on the land to be incinerated or ploughed into the soil with the disadvantages that this can result in: soil mineralization, air pollution and fire risks [11]. Biomass from olive-tree pruning can be used as fuel for heating systems in boilers [11,12], and its current price in Andalusia is 30-40 €/t while that of olive stone is 80-100 €/t, so that several industries in Spain are currently producing pellets from this lignocellulose material.

Water content in biomass is a key factor when the material is used for combustion. High moisture percentage increases the cost of transport and pelletizing, reduces the combustion efficiency and causes water vapour condensation, which can reduce the lifetime of boilers. Besides, during storage and handling of biomass, high moisture levels could promote microbial activity that is harmful to human health [13]. The monitoring of moisture level of biomass is of major importance to obtain high-quality pellets, the required water content for the pellet press being lower than 10%. Other thermo-chemical processes such as pyrolysis and gasification of biomass are normally carried out at low water contents [14,15]. For OS, an analysis of 15 samples collected from different factories in Andalusia showed that its moisture percentages ranged between 10.2% and 30.5%, with an average value of 22.3% [10], while some studies about OP reported moisture values in the range 30–35% [16]. Therefore, a drying operation should be applied to these biomasses before storage or other operations to reduce their moisture content to a suitable level.

Drying process occurs in several stages for high-moisture solid materials. During the initial stage (warming-up period) the rate of drying increases due to the temperature increase. In the second stage (constant-rate period) the surface of the solid is saturated with free water and the rate of moisture removal is constant and maximum. In the final stage of drying (falling-rate period), the area of the saturated surface gradually decreases when the water movement within the solid can no longer supply enough water to wet the surface. Therefore, the instantaneous drying rate continually decreases in this stage. The rate-controlling factors in the falling-rate period are complex, being water diffusion the predominant phenomenon in this stage [17]. Effective water diffusivity (D_{eff}) is an important drying parameter for biomass materials, useful for estimating drying times in the falling rate period and for designing and modelling the mass transfer during this period [18]. The D_{eff} value usually varies with the thickness of the material and the external drying conditions (gas temperature and rate). Several authors have applied Fick's second law of diffusion for D_{eff} values determination in by-products derived from olive grove. Thus, drying of wet olive pomaces has been researched at a wide range of temperatures (293–413 K) and sample thicknesses (7–63 mm) [19–21] while olive stone drying has only been studied at four temperatures (373, 423, 473 and 523 K) and three sample thicknesses (10, 20 and 30 mm) [22,23]. To the best of our knowledge, there are not works in the literature about D_{eff} determination in olive-tree pruning and the drying kinetics of OP has been not studied so far.

The two main objectives of the present study were: (a) to study the drying kinetics of both biomasses as a function of process time, air temperature and sample thickness and (b) to determine the effective water diffusivities during drying processes. These data would complete the available information on drying of biomasses derived from olive culture, which is of major importance for the design of dryers.

2. Materials and methods

2.1. Raw materials

The biomass samples used in this study were olive stone and olive-tree pruning. Olive stones, olive endocarps crushed into fragments, were collected from an olive oil mill (S.C.A. San Juan, Jaén province, Spain, UTM coordinates: 37º47´58.57´´N, 3º47´07.97´´W) and air-dried at room temperature (293±2 K) in laboratory for 10 days. These olive stones came from olives of the variety 'Picual'. Olive-tree prunings were collected on-site after fruit-harvesting from a ‘Picual’ olive grove situated in Alhama de Granada (Granada province, Spain, UTM coordinates: 37º01´59.08´´N, 3º56´10.80´´W). This biomass consisted of thin branches (< 5 cm diameter) and leaves. Leaves were removed from the woody fraction. The branches were air-dried at room temperature (293±2 K) in laboratory for 10 days and then grounded using a blade mill (Retsch, mod. SM1, Germany). Particle size distributions of OS and OP were determined using a vibratory screen (Restch, Mod. Vibro, Germany).

Prior to drying experiments, OS and OP were submerged in a distilled water bath at 293 K for 2 h and then submitted to gravity filtration for 15 min to obtain wet samples of olive stone (WOS) and wet samples of olive-tree pruning (WOP). Using 14 samples of each wet biomass, the moisture contents (wet basis) were found to be 22.9±1.0% and 51.4±3.3% for WOS and WOP, respectively.

2.2. Physical–chemical characterization of raw materials

2.2.1. Bulk density

Bulk density of biomass particles represents the ratio between the mass of biomass and its volume including the contribution of the interparticulate void volume. This physical property was determined according to a method previously described [24]. A glass graduated cylinder, with a total volume of 10 mL and an inner diameter of 16 mm, was used. A funnel filled with biomass was allowed to flow freely into the cylinder at a height of 160 mm. Solid mass in the container was determined using an electronic balance

(±0.001 g accuracy). Filling and weighing were repeated five times to calculate five values for bulk density.

2.2.2. Raw materials composition

Moisture content of the samples was analysed by drying in an oven at 378 K for 24 h (TAPPI T 264 cm-07). Extractives in raw materials were determined gravimetrically using a two-step sequential extraction process to remove water and ethanol soluble materials [25]. Determinations of structural carbohydrates (cellulose and hemicelluloses), acid-insoluble lignin (AIL) and acid soluble lignin (ASL) in raw materials were carried out using a two-step acid hydrolysis previously described [26]. Ash was determined according to TAPPI Standard Method T 15 os-58. All the analyses were carried out in duplicate.

2.2.3. Elemental analysis

Carbon, hydrogen, nitrogen and sulphur content in the raw materials were determined according to ASTM Standard method D5142-09 by using Thermo Finnigan Flash EA1112 CHNS-O Elemental Analyser. Oxygen content was calculated by subtraction of the CHNS content from the total content.

2.2.4. Higher heating value (HHV)

Higher heating value (HHV) of biomasses was measured by using an automatic Parr 6400 calorimeter. According to the results from elemental analysis, the value of HHV was also calculated by Demirbas' equation [27]:

$$\text{HHV (MJ/kg)} = 0.335\text{C} + 1.423\text{H} - 0.154\text{O} - 0.145\text{N} \quad (1)$$

where C, H, O and N are the weight percentages of carbon, hydrogen, oxygen and nitrogen in the biomass, respectively. Results were expressed as MJ/kg in dry weight basis.

2.2.5. Equilibrium moisture content (EMC)

Olive stones and olive-pruning debris were exposed to three constant levels of relative humidity at 282 K (43.1%, 57.4% and 77.5%) and 303 K (43.2%, 51.4% and 73.1%). Relative humidity was maintained by using the static gravimetric method and different saturated salt solutions (K_2CO_3, $Mg(NO_3)_2$ and $NaNO_3$), which can provide the respective humidity conditions [28]. Samples and salt solutions were maintained separately within a sealed container. The mass of each sample was initially weighed and then periodically removed, weighed and replaced in the container. Equilibrium was achieved when three consecutive weight measurements showed a difference of less than 1 mg. When equilibrium was reached, the samples were dried in an oven (378±1 K for 24 h) in order to obtain the dry matter content. All measurements were performed in duplicate.

2.3. Drying experiments and mathematical modelling of drying curves

The cabinet dryer (Selecta, Mod. 204, Barcelona, Spain) used for drying experiments had a height of 500 mm, a width of 400 mm and a depth of 450 mm. The dryer was composed of an electrical heater and a temperature controller. The relative humidity of the ambient air ranged from 50 to 70% during experiments. Drying experiments were performed by natural convection at 343, 353, 363, 373, 383 and 393 K for sample thicknesses of 25 and 50 mm. Furthermore, two additional assays were carried out at 393 K with sample thicknesses of 15 and 40 mm.

The samples were dried in 100-mL beakers (85 mm height and 46 mm internal diameter). For all test, weight variation with time was recorded by removing the beakers from the dryer, weighing them on a digital balance (±0.0001 g accuracy) and immediately returning them to the dryer. Each process of weight measurement lasted about 10 s. When drying process finished, the samples were dried in an oven (378±1 K for 24 h) in order to obtain the dry matter content. All drying experiments were performed in duplicate. The relative error was generally less than 7%. The standard deviation of the data is shown in the Figures.

Drying curves represent the moisture ratio (M_R) function versus drying time. The dimensionless moisture ratio for thin layer drying can be expressed as (Eq. 2):

$$M_R = (M_t - M_e)/(M_0 - M_e) \quad (2)$$

where M_t is the moisture content at a given time (kg water/kg dry matter), M_0 is the initial moisture content and M_e is the equilibrium moisture content. Since the values of M_e are small compared to M_t or M_0, the dimensionless moisture ratio could be expressed like,

$$M_R = M_t / M_0 \quad (3)$$

In our previous research [29], the experimental drying curves were fitted to six equations widely used to describe the kinetics of the drying process, namely, Lewis [30], Page [31], modified Page [32], Henderson and Pabis [33], logarithmic [34] and Midilli [35] models. These mathematical models for drying curves are illustrated in Table 1.

TABLE 1

Non-linear regression techniques were used to obtain the different constants in each selected model using the function 'Solver' in a Microsoft Excel spreadsheet. The coefficients of determination (r^2), reduced chi-squared (χ_r^2) and root mean square error (RMSE) were calculated to evaluate the fitting of each model to experimental data. The higher the values of r^2 and the lower the values of χ_r^2 and RMSE, the better the goodness of fit. These parameters can be calculated as,

$$r^2 = \sum_{i=1}^{N} \frac{\left(M_{R-pre,i} - \overline{M_{R-\exp,i}}\right)^2}{\left(M_{R-\exp,i} - \overline{M_{R-\exp,i}}\right)^2} \quad (4)$$

$$\chi_r^2 = \frac{\sum_{i=1}^{N}\left(M_{R-\exp,i} - M_{R-pre,i}\right)^2}{N-p} \quad (5)$$

$$RMSE = \left[\frac{1}{N}\sum_{i=1}^{N}\left(M_{R-pre,i} - M_{R-\exp,i}\right)^2\right]^{1/2} \quad (6)$$

where $M_{R\text{-}exp,i}$ is the experimental moisture ratio, $M_{R\text{-}pre,i}$ the predicted moisture ratio, N the number of data point and p is the number of constants in the regression model.

Tables S1, S2 and S3 illustrate, the fit values obtained for one particle size (50 mm) and 3 temperatures (70, 100 and 120 ºC). The two-parameter Page model and four-parameter Midilli model presented the best fit results [29]. However, Page model (Eq. 7) was selected for this work because of its better balance between accuracy and analytical simplicity,

$$M_R = \exp(-k\, t^n) \quad (7)$$

where t is drying time in hours, and k and n are empirical constants of the model.

3. Results and discussion

3.1. Biomasses

Olive stone and olive-tree pruning are two types of biomass with a high energetic potential in the European countries of the Mediterranean basin. Some physical, chemical and energetic properties of these materials are shown in Table 2. In relation to particle size distribution, OS had mainly diameters between 2 and 5 mm (73.9%, wt), and only 1.46% of the total particles weight corresponded to grains with diameters below 1.4 mm. For OP, 77.8% of the material had diameters between 1.030 and 1.400 mm after the grinding process carried out in laboratory.

The bulk density is a parameter with great importance in material handling and storage [36], and it was considerably higher for OS samples (721.6 ± 12.7 kg/m^3) than for OP samples (347.9 ± 13.4 kg/m^3). The bulk density value for olive stone is in agreement with that (693.0 ± 54.9 kg/m^3) reported by other authors [10].

The structural composition of OS and OP is shown in Table 2. Both biomasses were mainly composed of cellulose, hemicelluloses and lignin. The percentages of hemicelluloses and lignin were higher for OS, while cellulose was higher for OP. The rest corresponded to extractives, which include non-structural sugars, tannins and chlorophyll, and mineral salts. Elemental analysis results showed that OS and OP were mainly composed of carbon (49.7% and 44.4%, respectively) and oxygen (43.4% and 48.3%, respectively). Besides, negligible values of sulphur and low percentages of nitrogen (0.128% and 0.771%, respectively) were found, which is important from an environmental point of view because it contributes to lowering SOx and NOx emissions.

With regards to higher heating values (HHV) obtained from tests in the calorimeter, OS and OP samples reached values of 18.8 and 17.4 MJ/kg, respectively (Table 2). These data indicate that OS and OP have a great potential as solid biofuels in combustion processes, being the potential of OS higher due to its higher HHV and bulk density. The predicted HHV by Demirbas' equation (19.7 MJ/kg for OS and 16.7 MJ/kg for OP) agreed well with the experimental results.

The equilibrium moisture content (EMC) can be used as an indicator of hydrophobicity of a solid. EMC of olive stone and olive-tree pruning was measured at 283 and 303 K with relative humidity (RH) ranging from 43.1% to 77.5% (Table 2). For a given material, the EMC increased with RH and decreased with an increase in the temperature. Depending on the RH values and temperatures, the EMC ranged from 9.13% to 13.3% for OS and from 10.1% to 15.5% for OP. Data from Table 2 shows that OP is slightly more hydrophilic than OS, probably due to the higher porosity of the olive wood. The differences in EMC values also could be related with cell wall compositions, especially with water-extractives (hydrophilic materials) and lignin (hydrophobic material) percentages. The EMC values were similar than those reported at 293 K for willow (EMC = 12.5% for RH = 75.0%) [37], and at 288 K for miscanthus stems (EMC = 15.0% for RH = 75.6%) [38].

TABLE 2

3.2. Mathematical modelling of drying curves

The experimental drying curves of wet olive stone and olive-tree pruning (WOS and WOP, respectively) for different values of drying air temperature and sample thickness are shown in Fig. 1. As expected, the moisture content decreased continuously with drying time for all assays. Furthermore, an increase in temperature and a decrease in sample thickness resulted in reduced drying time of the two biomasses. The drying times to reach a moisture content of 10% (wet basis) working with 50 mm sample thickness at 343, 373 and 393 K were 13.4, 6.2 and 2.8 h for WOS, and 22.0, 9.5 and 6.3 h for WOP, respectively. The shortest drying times were obtained at 393 K using a sample thickness of 15 mm: 1.0 h for WOS and 1.6 h for WOP.

For comparison with experimental data, calculated moisture contents from Page model (Eq. 7) are also shown in Fig. 1. The values of k and n coefficients of model are summarised in Table 3 along with values obtained for r^2 (0.996–0.999), χ_r^2 (1.82×10^{-5} –9.07×10^{-4}) and RMSE values (0.0037–0.0246), indicating a good fit.

FIGURE 1

TABLE 3

The previous results show the suitability of the Page model to describe the drying behaviour of wet olive stone and olive-tree pruning. However, this model does not reproduce the influence of drying temperature. The experimental data obtained for thickness sample of 50 mm were used to assess the dependence of k and n with drying temperature. The experimental n values had not a high variability with temperature (Table 3) and it could be defined by means of a uniform exponent (n = 1.44±0.13 for WOS, and n = 1.81±0.06 for WOP) as the average of all n values. On the other hand, the k coefficients dependence with temperature can be described by an Arrhenius-type equation. Thus, the following mathematical formulas were proposed to evaluate the moisture ratio of the two biomasses at the drying times (h) and air temperatures (K) assayed:

$$\ln M_R = -\exp[8.954 - (4286.613/T)]\, t^{1.439} \tag{8}$$

for WOS, and

$$\ln M_R = -\exp[10.780 - (5260.929/T)]\, t^{1.810} \tag{9}$$

for WOP.

Figure 2 shows the comparison between experimental and predicted values of M_R calculated using the new mathematical models (Eqs. 8 and 9), indicating good fits to the experimental data, especially for wet olive-tree pruning (r^2 = 0.992, χ_r^2 = 1.07 × 10^{-3} and RMSE = 0.0324). Considering the whole range of assayed temperatures (343-393 K), the value of r^2 for olive stone is relatively low (r^2 = 0.982), but it markedly improves (r^2 = 0.994, χ_r^2 = 1.34 × 10^{-3} and RMSE = 0.0361) when excluding the data obtained at 373 K (i.e. using the drying temperatures between 343 and 383 K).

FIGURE 2

3.3. Drying rates (D_R)

In order to deepen the knowledge about the drying processes, the experimental drying rates (D_R) for WOS and WOP were calculated by Eq. (10),

$$D_R = \frac{\mathrm{d}(M_R)}{\mathrm{d}t} \approx \frac{(M_R)_{t+\Delta t} - (M_R)_t}{\Delta t} \tag{10}$$

where t is the drying time and $(M_R)_{t+\Delta t}$ and $(M_R)_t$ stand for the moisture content at times ($t+\Delta t$) and t, respectively.

Fig. 3 depicts the relation between D_R and time, and between D_R and moisture ratio, for experiments carried out in the range 343–393 K with 50 mm of sample thickness. The figure also shows the predicted values of drying rate calculated from the time derivative of Eq. (7) using the values of k and n tabulated in Table 3. It can be stated that the Page model gives an adequate estimation of drying rates for experiments performed between 343 K and 383 K. However, errors were considerable at 393 K, especially for wet olive-tree pruning.

The analysis of drying rates allowed determining the number of stages and their characteristics during the drying of biomasses. Warming-up period was observed at the beginning of all drying processes, and it was longer for WOP than for WOS. For both biomasses, this period increased when increasing drying temperature, which is in agreement with previous studies [22].

The constant drying period (CDP) was not observed for WOS under any drying condition. However, this stage was found working with WOP for some temperatures and samples thicknesses such as at 353 K and 50 mm thicknesses (Fig. 4). Experimental data indicated that, for a fixed temperature, the decrease of sample thickness led, on the one hand, to an increase of warming-up period and, on the other hand, to the reduction or even the disappearance of the constant drying period. This behaviour can be clearly observed in Fig. 4 for WOP thicknesses of 25 and 50 mm. The presence of constant drying periods for WOP could be explained taking into account that this biomass had smaller particle sizes than olive stone (Table 2) which could imply higher interface area per volume of packed bed. The increase in the sample thickness from 25 to 50 mm does not change the sample surface in contact with the external drying air (S_{CDA}) but increases the volume of packed bed, so the internal moisture transfer could be sufficient to maintain S_{CDA} saturated for a long time. Air temperature and sample thickness had a significant effect on the maximum drying rate ($D_{R,\max}$) for both WOS and WOP. Thus, $D_{R,\max}$ increased from 0.0598 h^{-1} to 0.225 h^{-1} for WOS, and from 0.057 h^{-1} to 0.170 h^{-1} for WOP when thickness was set to 50 mm and the process temperature was increased from 343 K to 393 K (Fig. 3). For a sample thickness of 25 mm at the same range of temperatures (343–393 K) the $D_{R,\max}$ values ranged from 0.151 to 0.390 h^{-1} and from 0.146 to 0.323 h^{-1} for WOS and WOP, respectively. The highest values of maximum drying rate were achieved at 393 K with a sample thickness of 15 mm: 0.739 h^{-1} for WOS and 0.776 h^{-1} for WOP. The calculated value of $D_{R,\max}$ for wet olive stone (0.739 h^{-1}) is consistent with those (0.72 and 1.08 h^{-1}) obtained by other authors [22] for the drying of olive stone with thickness of 20 mm at 373 and 423 K, respectively. With regard to OP, since its drying kinetics has been not previously studied, no comparison with other authors' results could be performed.

FIGURE 3

FIGURE 4

3.4. Effective diffusivity

During the falling-rate period, the drying rate begins to fall because the rate of moisture transfer from the interior of the packed bed towards external surface is lower than the rate of evaporation from that surface. In this stage, the drying process is controlled by the molecular transport of moisture which occurs according to a concentration gradient of water across the packed bed. Therefore, experimental results could be interpreted by using Fick's second law of diffusion (Eq. (11)),

$$\frac{\mathrm{d}C}{\mathrm{d}t} = D\frac{\mathrm{d}^2C}{\mathrm{d}x^2} \tag{11}$$

where C is the water concentration, D is the diffusion coefficient and x is the distance in the flow direction.

An analytical solution to the differential equation has been established for the one-dimensional mass transport in infinite slab geometry under the following limitations [39]: isothermal drying conditions, constant effective diffusivity, and negligible shrinkage and external resistance (Eq. (12)),

$$M_R = \frac{8}{\pi^2} \sum_{n=0}^{\infty} \frac{1}{(2n+1)^2} \exp\left(- \frac{(2n+1)^2 \pi^2 D_{\text{eff}} t}{4L^2} \right) \tag{12}$$

where D_{eff} is the effective diffusivity, n is the number of terms taken into consideration, L is the thickness of slab and t is the drying time.

For long drying periods, Eq. (12) can be simplified to the first term of the series,

$$M_R = \frac{8}{\pi^2} \exp\left(- \frac{\pi^2 D_{\text{eff}} t}{4L^2} \right) \tag{13}$$

Eq. (13) can be linearized in the following way,

$$\ln M_R = \ln \frac{8}{\pi^2} - \frac{\pi^2 D_{\text{eff}} t}{4L^2} \tag{14}$$

From the representation of the first member ($\ln M_R$) against time (t), the effective water diffusivity (D_{eff}) can be determined from the slope ($-\pi^2 D_{\text{eff}} 4^{-1} L^{-2}$) (Fig. 5).

FIGURE 5

Values of D_{eff} for each experiment along with the coefficients of determination r^2 are shown in Table 4. This table illustrates that, under the same experimental conditions, effective water diffusivities through WOS (between 1.87×10^{-8} m^2/s and 16.4×10^{-8} m^2/s) were lower than though WOP (between 3.41×10^{-8} m^2/s and 32.5×10^{-8} m^2/s). What is more, diffusivities for wet olive-tree pruning were roughly twice than those measured with wet olive stone (Fig. 6). It can be seen that the D_{eff} values obtained in the present study are in agreement with those obtained for the drying of olive cake (6.80×10^{-8} m^2/s to 21.5×10^{-8} m^2/s) at temperatures between 323 and 353 K [20] or coconut (5.99×10^{-8} m^2/s to 26.6×10^{-8} m^2/s) in the range 333–393 K [40]. Similar D_{eff} values of 1.64×10^{-8} m^2/s and 3.13×10^{-8} m^2/s for the drying process of olive stone at 373 K and 423 K, respectively, have been previously reported [22]. By contrast, there is not available data in literature for WOP. Data from Table 4 also indicates that D_{eff} values increased notably with air temperature. Thus, when WOS with 25 mm thickness were dried, the D_{eff} values continuously increased from 1.87×10^{-8} m^2/s to $6.34\cdot 10^{-8}$ m^2/s when air temperature rose from 343 K to 393 K. The same trend was observed when sample thickness was 50 mm and also in the experiments with WOP. On the other hand, results showed a general trend of increasing effective diffusivity with decreasing sample thickness. Thus, for WOP at 393 K and sample thicknesses of 15 mm, 25 mm, 40 mm and 50 mm, the effective water diffusivities were 12.0×10^{-8} m^2/s, 13.0×10^{-8} m^2/s, 30.2×10^{-8} m^2/s and 32.5×10^{-8} m^2/s, respectively, while for WOS under the same experimental conditions (393 K temperature, and 15 mm, 25 mm, 40 mm and 50 mm thickness) the effective water diffusivities were 7.22×10^{-8} m^2/s, 6.34×10^{-8} m^2/s, 15.4×10^{-8} m^2/s and 16.4×10^{-8} m^2/s, respectively. This behaviour has been reported by other authors working with olive stone [22].

TABLE 4

FIGURE 6

In diffusion of solids, the temperature dependence of the effective diffusion coefficient (D_{eff}) of water through the solid can be described by an empirical equation (Eq. (15)), which has the typical form describing an activated process [41],

$$D_{eff} = \alpha \exp\left(-\frac{\beta}{T}\right) \quad (15)$$

where α (m^2/s) and β (K) are empirical constants and T is the absolute temperature (K).

Therefore, the values of α and β were calculated by plotting the natural logarithm of D_{eff} versus the reciprocal of the absolute temperature, as presented in Fig. 7, where the coefficients of determination values are also shown.

FIGURE 7

4. Conclusions

This study confirms that olive stone exhibits better energetic characteristics for combustion process than olive-tree pruning, because of its higher gross calorific value (18.8 *vs* 17.4 MJ/kg) and bulk density (721.6 *vs* 347.9 kg/m^3), and its lower ash percentage (0.69 *vs* 2.7%). By contrast, its current price (80-100 €/t) is more than twice higher than that of olive-tree pruning (30-40 €/t), which can be a hindrance for industrial applications.

With regards to the drying process of wet olive stone, no constant rate period was observed, and the water loss was mainly accomplished during the falling rate period. By contrast, wet olive-tree pruning showed constant drying period under some experimental conditions, which could be related to the smaller particle size obtained for this biomass after grinding. Temperature increase and sample thickness decrease resulted in a reduction of the drying time for both biomasses, the highest drying rates being achieved at the maximum temperature (393 K) and sample thickness (15 mm) assayed (0.739 h^{-1} for wet olive stone and 0.776 h^{-1} for wet olive-tree pruning). Page Model was successfully applied for drying kinetics prediction and two new mathematical equations were proposed to describe the dependence of moisture ratio with drying time and temperature.

The values of effective water diffusivity, calculated at the falling rate period, increased when the drying temperature and the sample thickness rose as well. Diffusion coefficient values for olive-tree pruning (between 3.4×10^{-8} m^2/s and 32.5×10^{-8} m^2/s), which have been for first time determined in this work, were almost twice as high as those for olive stone (between 1.87×10^{-8} m^2/s and 16.4×10^{-8} m^2/s). These differences can lead to modifications in the design of rotary dryers for these biomasses.

Acknowledgments

The authors would like to acknowledge to the olive oil mill ‘S.C.A. San Juan’ (Jaén, Spain) and to the farm ‘El boje’ for supply of olive stones and olive-pruning debris, respectively. Furthermore, the authors also thank to Andalusia Regional Government for financial support, Project AGR/6509, and to CICT of University of Jaén (Junta de Andalucía–MINECO–FEDER) for the technical support provided.

References

[1] C. Europeia, REPORT FROM THE COMMISSION TO THE COUNCIL AND THE EUROPEAN PARLIAMENT on sustainability requirements for the use of solid and gaseous biomass sources in electricity, heating and cooling, 2010. doi:SEC(2010) 65; SEC(2010) 66.

[2] M. Cuevas, S. Sánchez, J.F. García, Thermochemical and biochemical conversion of olive stones, in: C.N. Foster (Ed.), Agric. Wastes Charact. Types

Manag., Nova Science Publishers, 2015: pp. 61–86.

[3] C. Galán, H. García-Mozo, L. Vázquez, L. Ruiz, C. Díaz De La Guardia, E. Domínguez-Vilches, Modeling olive crop yield in Andalusia, Spain, Agron. J. 100 (2008) 98–104. doi:10.2134/agronj2006.0345.

[4] J. Gómez, J. Infante-Amate, M. de Molina, T. Vanwalleghem, E. Taguas, I. Lorite, Olive cultivation, its impact on soil erosion and its progression into yield impacts in Southern Spain in the past as a key to a future of increasing climate uncertainty, Agriculture. 4 (2014) 170–198. doi:10.3390/agriculture4020170.

[5] A. Roig, M.L. Cayuela, M.A. Sánchez-Monedero, An overview on olive mill wastes and their valorisation methods, Waste Manag. 26 (2006) 960–969. doi:10.1016/j.wasman.2005.07.024.

[6] M. Cuevas, S. Sánchez, J.F. García, J. Baeza, C. Parra, J. Freer, Enhanced ethanol production by simultaneous saccharification and fermentation of pretreated olive stones, Renew. Energy. 74 (2015) 839–847. doi:10.1016/j.renene.2014.09.004.

[7] T.M. Alslaibi, I. Abustan, M.A. Ahmad, A.A. Foul, Application of response surface methodology (RSM) for optimization of Cu2+, Cd2+, Ni2+, Pb2+, Fe2+, and Zn2+ removal from aqueous solution using microwaved olive stone activated carbon, J. Chem. Technol. Biotechnol. 88 (2013) 2141–2151. doi:10.1002/jctb.4073.

[8] D. Montané, J. Salvadó, C. Torras, X. Farriol, High-temperature dilute-acid hydrolysis of olive stones for furfural production, Biomass and Bioenergy. 22 (2002) 295–304. doi:10.1016/S0961-9534(02)00007-7.

[9] G. Rodríguez, A. Lama, M. Trujillo, J.L. Espartero, J. Fernández-Bolaños, Isolation of a powerful antioxidant from Olea europaea fruit-mill waste: 3,4-

Dihydroxyphenylglycol, LWT - Food Sci. Technol. 42 (2009) 483–490. doi:10.1016/j.lwt.2008.08.015.

[10] J. Mata-Sánchez, J.A. Pérez-Jiménez, M.J. Díaz-Villanueva, A. Serrano, N. Núñez-Sánchez, F.J. López-Giménez, Development of olive stone quality system based on biofuel energetic parameters study, Renew. Energy. 66 (2014) 251–256. doi:10.1016/j.renene.2013.12.009.

[11] J.F. García, S. Sánchez, J. García, Ethanol from biomass: Application to the olive-pruning debris, in: D.A. Carasillo (Ed.), Liq. Fuels Types, Prop. Prod., Nova Science Publishers, 2012: pp. 239–254.

[12] F.J. Lopez, S. Pinzi, J.J. Ruiz, A. Lopez, M.P. Dorado, Economic viability of the use of olive tree pruning as fuel for heating systems in public institutions in South Spain, Fuel. 89 (2010) 1386–1391. doi:10.1016/j.fuel.2009.11.003.

[13] T. Gebreegziabher, A.O. Oyedun, C.W. Hui, Optimum biomass drying for combustion - A modeling approach, Energy. 53 (2013) 67–73. doi:10.1016/j.energy.2013.03.004.

[14] R. Moreno, G. Antolín, A. Reyes, P. Alvarez, Drying characteristics of forest biomass particles of Pinus radiata, Biosyst. Eng. 88 (2004) 105–115. doi:10.1016/j.biosystemseng.2004.02.005.

[15] Y. Huangfu, H. Li, X. Chen, C. Xue, C. Chen, G. Liu, Effects of moisture content in fuel on thermal performance and emission of biomass semi-gasified cookstove, Energy Sustain. Dev. 21 (2014) 60–65. doi:10.1016/j.esd.2014.05.007.

[16] R. Spinelli, G. Picchi, Industrial harvesting of olive tree pruning residue for energy biomass, Bioresour. Technol. 101 (2010) 730–735. doi:10.1016/j.biortech.2009.08.039.

[17] R. Perry, D. Green, J. Maloney, Perry’s chemical engineers’ handbook, 1997.

doi:10.10360071422943.

[18] J. Srikiatden, J.S. Roberts, Moisture transfer in solid food materials: A review of mechanisms, models, and measurements, Int. J. Food Prop. 10 (2007) 739–777. doi:10.1080/10942910601161672.

[19] I. Montero, T. Miranda, J.I. Arranz, C.V. Rojas, Thin layer drying kinetics of by-products from olive oil processing, Int. J. Mol. Sci. 12 (2011) 7885–7897. doi:10.3390/ijms12117885.

[20] S. Meziane, Drying kinetics of olive pomace in a fluidized bed dryer, Energy Convers. Manag. 52 (2011) 1644–1649. doi:10.1016/j.enconman.2010.10.027.

[21] A. Ruiz Celma, S. Rojas, F. Lopez-Rodríguez, Mathematical modelling of thin-layer infrared drying of wet olive husk, Chem. Eng. Process. Process Intensif. 47 (2008) 1810–1818. doi:10.1016/j.cep.2007.10.003.

[22] F.J. Gómez-de la Cruz, P.J. Casanova-Peláez, J.M. Palomar-Carnicero, F. Cruz-Peragón, Drying kinetics of olive stone: A valuable source of biomass obtained in the olive oil extraction, Energy. 75 (2014) 146–152. doi:10.1016/j.energy.2014.06.085.

[23] F.J. Gómez-De La Cruz, J.M. Palomar-Carnicero, P.J. Casanova-Peláez, F. Cruz-Peragón, Experimental determination of effective moisture diffusivity during the drying of clean olive stone: Dependence of temperature, moisture content and sample thickness, Fuel Process. Technol. 137 (2015) 320–326. doi:10.1016/j.fuproc.2015.03.018.

[24] P.S. Lam, S. Sokhansanj, X.T. Bi, C.J. Lim, S.H. Larsson, Drying characteristics and equilibrium moisture content of steam-treated Douglas fir (Pseudotsuga menziesii L.), Bioresour. Technol. 116 (2012) 396–402. doi:10.1016/j.biortech.2012.03.093.

[25] A. A. Sluiter, R. Ruiz, C. Scarlata, J. Sluiter, D. Templeton, Determination of Extractives in Biomass: Laboratory Analytical Procedure (LAP); Issue Date 7/17/2005 - 42619.pdf, Tech. Rep. NREL/TP-510-42619. (2008) 1–9. doi:NREL/TP-510-42621.

[26] M. Cuevas, J.F. García, S. Sánchez, Enhanced enzymatic hydrolysis of pretreated almond-tree prunings for sugar production, Carbohydr. Polym. 99 (2014) 791–799. doi:10.1016/j.carbpol.2013.08.089.

[27] A. Demirbas, Calculation of higher heating values of fatty acids, Energy Sources, Part A Recover. Util. Environ. Eff. 38 (2016) 2693–2697. doi:10.1080/15567036.2015.1115924.

[28] L. Greenspan, Humidity fixed points of binary saturated aqueous solutions, J. Res. Natl. Bur. Stand. Sect. A Phys. Chem. 81A (1977) 89. doi:10.6028/jres.081A.011.

[29] L. Hernández, Estudio del secado de hueso de aceituna y poda de olivar para mejorar su uso como biocombustibles en calderas de biomasa, University of Jaén, 2015.

[30] W.K. Lewis, The Rate of Drying of Solid Materials, Ind. Eng. Chem. 13 (1921) 427–432. doi:10.1021/ie50137a021.

[31] G.E. Page, Factors influencing the maximum rates of air drying shelled corn in thin layers, Purdue University, 1949.

[32] D.G. Overhults, G.M. White, H.E. Hamilton, I.J. Ross, Drying Soybeans With Heated Air, Trans. ASAE. 16 (1973) 112–113. doi:10.13031/2013.37459.

[33] S.M. Henderson, S. Pabis, Grain drying theory II: Temperature effects on drying coefficients, J. Agric. Eng. Res. (1961) 169–174.

[34] I.T. Togrul, D. Pehlivan, Mathematical modelling of solar drying of apricots in

thin layers, J. Food Eng. 55 (2002) 209–216. doi:10.1016/S0260-8774(02)00065-1.

[35] A. Midilli, H. Kucuk, Z. Yapar, A new model for single layer drying, Dry. Technol. 20 (2002) 1503–1513. doi:10.1081/drt-120005864.

[36] Z. Liu, B. Mi, Z. Jiang, B. Fei, Z. Cai, X. Liu, Improved bulk density of bamboo pellets as biomass for energy production, Renew. Energy. 86 (2016) 1–7. doi:10.1016/j.renene.2015.08.011.

[37] B. Krupinska, I. Strømmen, Z. Pakowski, T.M. Eikevik, Modeling of sorption isotherms of various kinds of wood at different temperature conditions, Dry. Technol. 25 (2007) 1459–1466. doi:10.1080/07373930701537062.

[38] J.J. Fitzpatrick, C. O'Sullivan, H. Boylan, O. Cribben, D. Costello, K. Cronin, Moisture sorption isotherm study of Sitka spruce, larch, willow and miscanthus chips and stems, Biosyst. Eng. 115 (2013) 474–481. doi:10.1016/j.biosystemseng.2013.05.004.

[39] J. Crank, The mathematics of diffusion, Clarendon Press, Oxford, England, 1975.

[40] T. Madhiyanon, A. Phila, S. Soponronnarit, Models of fluidized bed drying for thin-layer chopped coconut, Appl. Therm. Eng. 29 (2009) 2849–2854. doi:10.1016/j.applthermaleng.2009.02.003.

[41] C.O. Bennett, J.E. Myers, Molecular diffusion and diffusivity, in: Momentum, Heat, and Mass Transfer, McGraw-Hill (2ª Ed.), New York, 1974.

Table 1

Mathematical models of drying curves.

Model name	Equation	References
Lewis	$M_R = \exp(-kt)$	[30]
Page	$M_R = \exp(-kt^n)$	[31]
Modified Page	$M_R = \exp(-(kt)^n)$	[32]
Henderson and Pabis	$M_R = a \exp(-kt)$	[33]
Logarithmic	$M_R = a \exp(-kt) + c$	[34]
Midilli et al.	$M_R = a \exp(-kt^n) + bt$	[35]

Table 2

Physicochemical properties of dry olive stone (OS) and olive-tree pruning (OP)

Property		OS	OP
Particle size (mm), %	5.00 > x > 2.00	73.905	0.086
	2.00 > x > 1.80	16.330	0.125
	1.80 > x > 1.40	8.313	7.448
	1.40 > x > 1.03	1.105	77.798
	1.03 > x > 0.730	0.245	12.673
	0.730 > x > 0.510	0.074	1.432
	0.510 > x > 0.360	0.012	0.280
	0.360 > x > 0.210	0.016	0.157
	0.210 > x	0.000	0.000
Bulk density, kg/m^3		721.6±12.7	347.9±13.4
Composition	Extractives, %	6.01±0.06	19.5±0.1
	Cellulose, %	26.1±0.3	29.4±0.5
	Hemicelluloses, %	26.3±0.5	20.3±0.2
	AIL, %	31.3±0.8	20.2±0.7
	ASL,%	2.12±0.22	0.41±0.07
	Ash, %	0.691±0.031	2.67±0.18
Elemental analysis	C, %	49.7±0.1	44.4±0.0
	H, %	6.83±0.09	6.62±0.14
	N, %	0.128±0.002	0.771±0.042
	S, %	n.d.	n.d.
	O, %	43.4±0.0	48.3±0.2
High heating value	Calorimetric pump, MJ/kg	18.8±0.2	17.4±0.1
	Demirbas equation, MJ/kg	19.7±0.1	16.7±0.2
EMC (283 K), % d.b.	RH = 43.1%	10.6	11.4
	RH = 57.4%	11.5	11.9
	RH = 77.5%	13.3	15.5
EMC (303 K), % d.b.	RH = 43.2%	9.13	10.1
	RH = 51.4%	10.3	11.7
	RH = 73.1%	11.5	12.3

AIL: Acid Insoluble Lignin; ASL: Acid Soluble Lignin. n.d.: not detected; EMC: Equilibrium Moisture Content; RH: Relative Humidity.

Table 3
Statistics for the Page model. Influence of temperature and sample thickness.

Biomass	*ST* (mm)	*T* (K)	Coefficient *k* (h^{-1})	Coefficient *n*	r^2	χ_r^2	RMSE
WOS	15	393	1.01	1.84	1.00	7.52×10^{-5}	0.00733
	25	343	0.0474	1.67	0.998	2.75×10^{-4}	0.0156
		353	0.207	1.16	0.999	1.55×10^{-4}	0.0110
		363	0.234	1.24	0.999	1.58×10^{-4}	0.0112
		373	0.217	1.50	1.00	5.94×10^{-5}	0.00680
		383	0.277	1.51	0.999	2.67×10^{-4}	0.0138
		393	0.503	1.40	1.00	1.82×10^{-5}	0.00370
	40	393	0.349	1.40	1.00	2.22×10^{-5}	0.00408
	50	343	0.0295	1.35	1.00	4.99×10^{-5}	0.00673
		353	0.0538	1.29	1.00	4.68×10^{-5}	0.00647
		363	0.0491	1.44	1.00	3.36×10^{-5}	0.00536
		373	0.0698	1.45	0.999	7.83×10^{-5}	0.00819
		383	0.0693	1.67	0.999	1.89×10^{-4}	0.0124
		393	0.223	1.43	1.00	2.98×10^{-5}	0.00502
WOP	15	393	0.781	2.36	0.997	9.07×10^{-4}	0.0246
	25	343	0.0153	2.19	0.999	1.57×10^{-4}	0.0116
		353	0.0376	2.01	0.998	5.04×10^{-4}	0.0207
		363	0.0811	1.95	0.999	1.87×10^{-4}	0.0121
		373	0.122	1.86	0.997	5.56×10^{-4}	0.0199
		383	0.112	2.19	0.999	2.51×10^{-4}	0.0134
		393	0.257	1.93	0.999	2.68×10^{-4}	0.0134
	40	393	0.137	1.73	0.997	6.26×10^{-4}	0.0217
	50	343	0.00953	1.77	1.00	4.91×10^{-5}	0.00648
		353	0.0163	1.76	0.998	2.59×10^{-4}	0.0152
		363	0.0303	1.76	1.00	1.82×10^{-5}	0.00398
		373	0.0368	1.82	0.998	2.75×10^{-4}	0.0154
		383	0.0461	1.91	0.999	3.78×10^{-4}	0.0176
		393	0.0744	1.86	0.996	5.18×10^{-4}	0.0212

ST: Sample thickness; WOS: Wet olive stone; WOP: Wet olive-tree pruning. χ_r^2: Reduced chi-square; RMSE: Root mean square error.

Table 4
Effective moisture diffusivity (D_{eff}) for each experimental condition.

		Wet olive stone		Wet olive-tree pruning	
ST (mm)	*T* (K)	$D_{eff} \times 10^8$ (m^2/s)	r^2	$D_{eff} \times 10^8$ (m^2/s)	r^2
15	393	7.22	0.996	12.0	0.978
25	343	1.87	0.999	3.41	0.998
	353	2.24	0.993	4.51	0.991
	363	3.14	0.992	6.09	0.995
	373	3.96	0.992	7.60	0.995
	383	5.18	0.994	10.4	0.999
	393	6.34	0.994	13.0	0.994
40	393	15.4	0.991	30.2	0.984
50	343	3.46	0.996	4.95	0.996
	353	4.59	0.998	7.59	0.996
	363	6.07	0.999	9.96	0.999
	373	7.66	0.999	15.7	0.991
	383	12.1	0.992	22.3	0.980
	393	16.4	0.997	32.5	0.991

ST: Sample thickness.

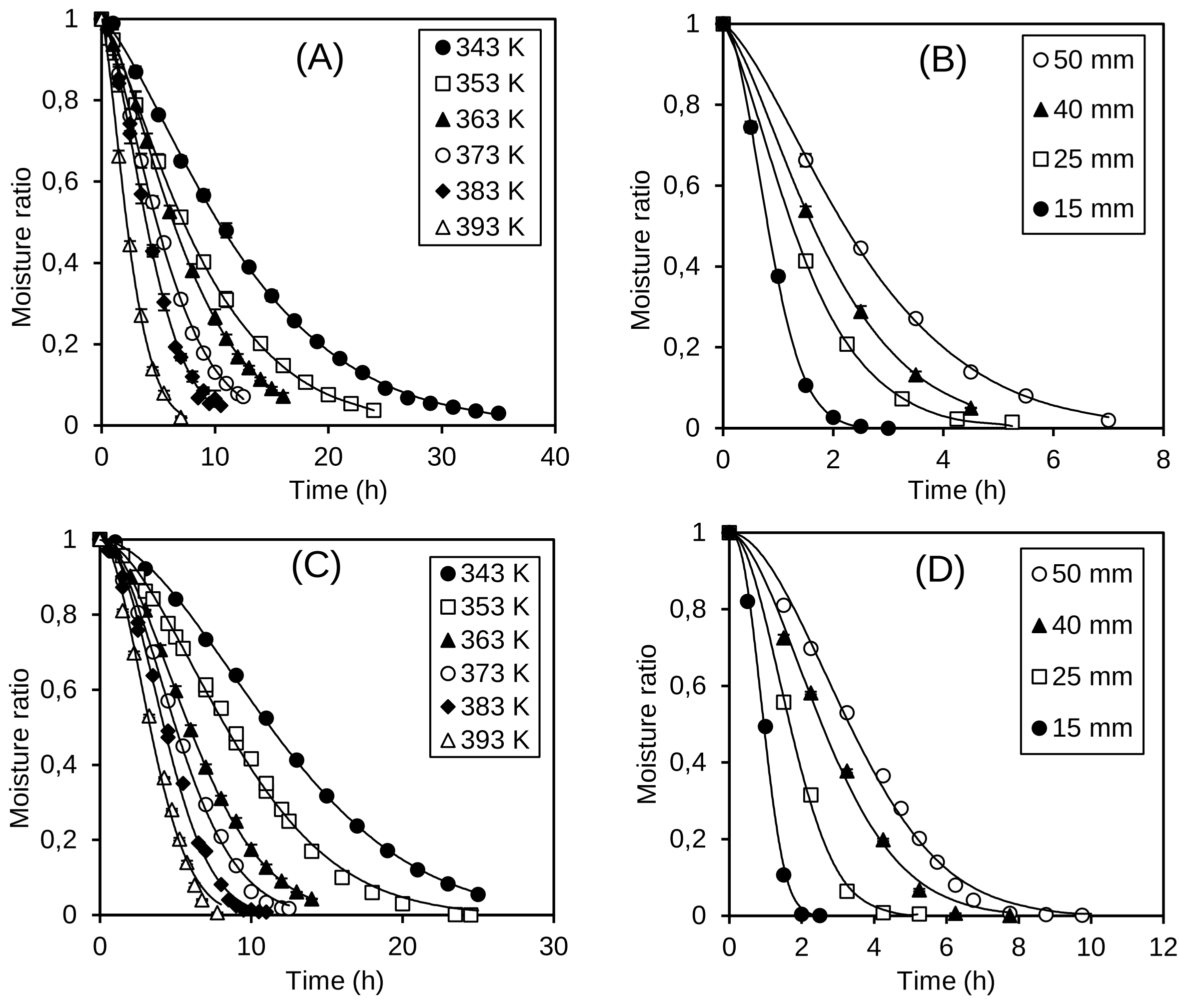

Fig. 1. Drying curves of WOS (A, B) and WOP (C, D) at different temperatures (A, C, sample thickness: 50 mm) and sample thicknesses (B, D, temperature: 393 K). Points: experimental data. Lines: predicted data by Page model.

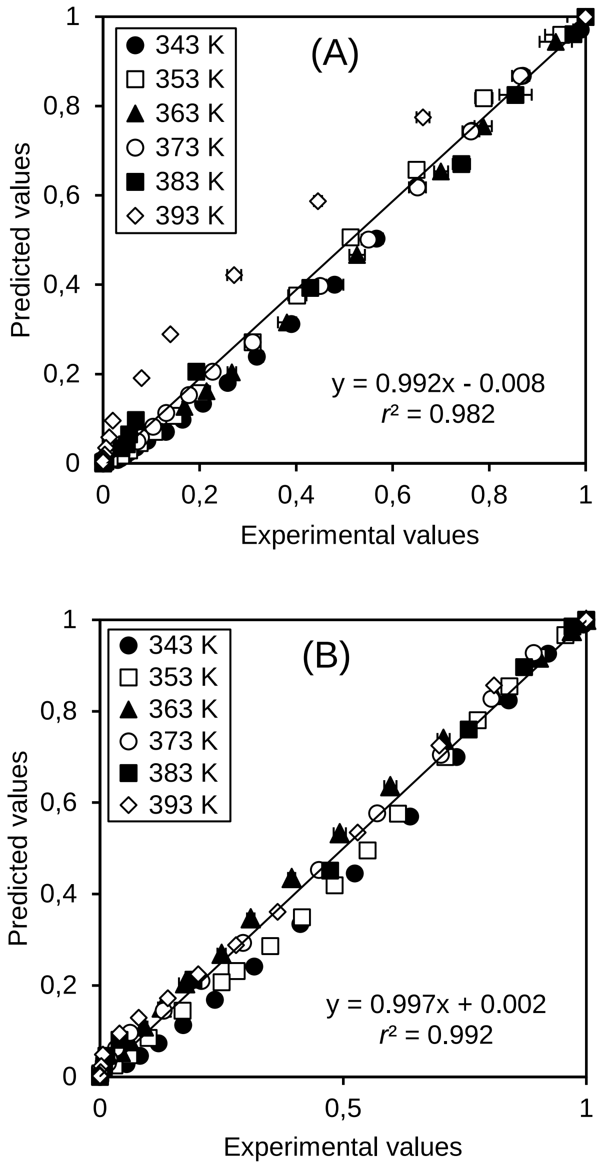

Fig. 2. Experimental and predicted moisture ratio values according to Eqs. (8) and (9) for WOS (A) and WOP (B), respectively. Sample thickness: 50 mm.

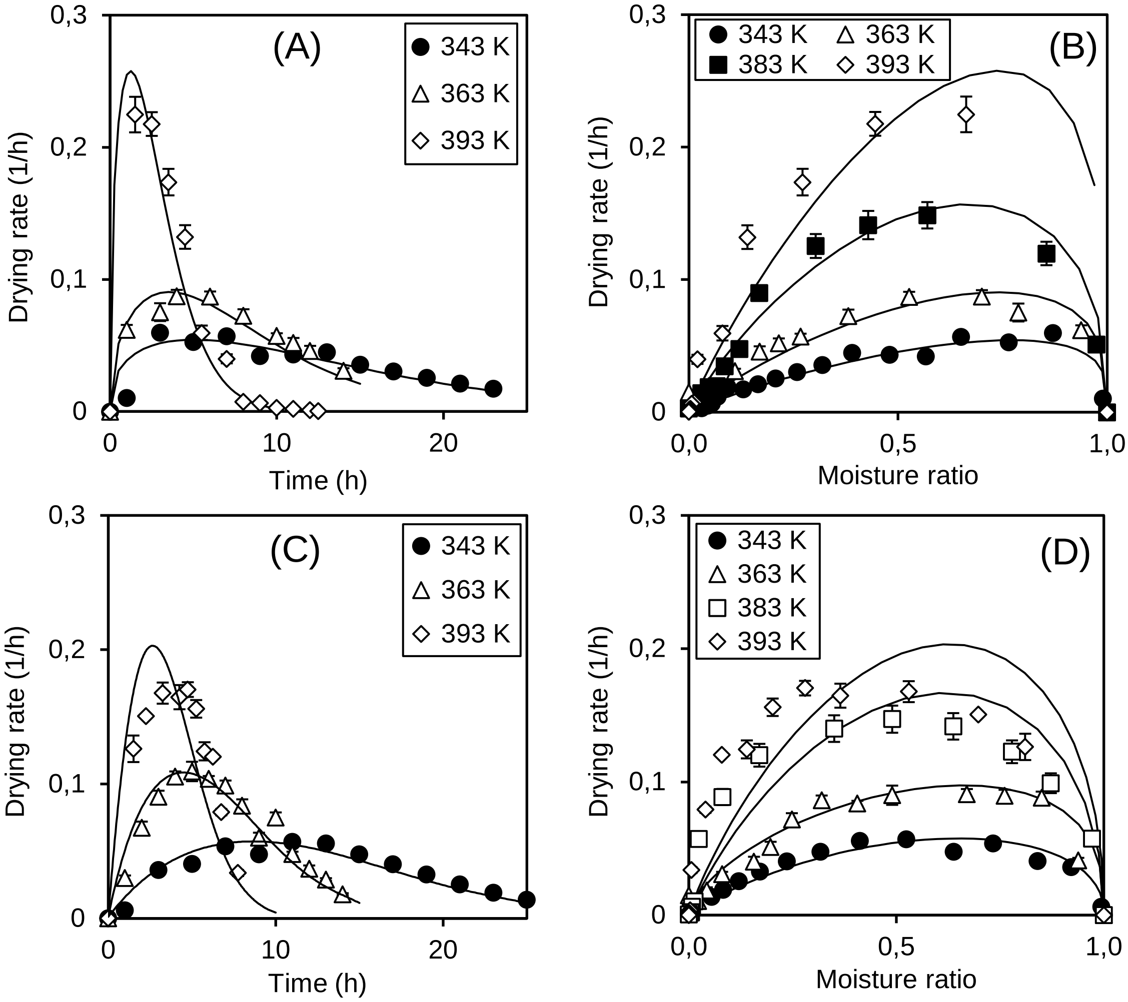

Fig. 3. Drying rate of OS (A, B) and OP (C, D) *vs* drying time and moisture ratio at different temperatures (sample thickness: 50 mm). Lines: Page model.

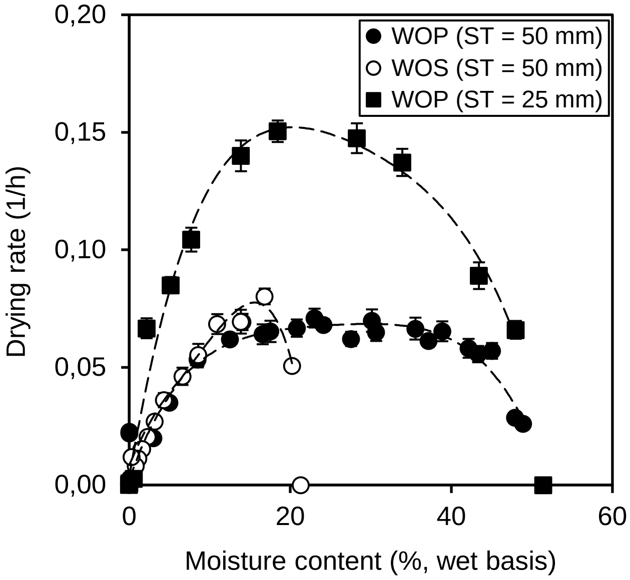

Fig. 4. Profile of drying rate versus moisture content at 353 K for WOS and WOP.

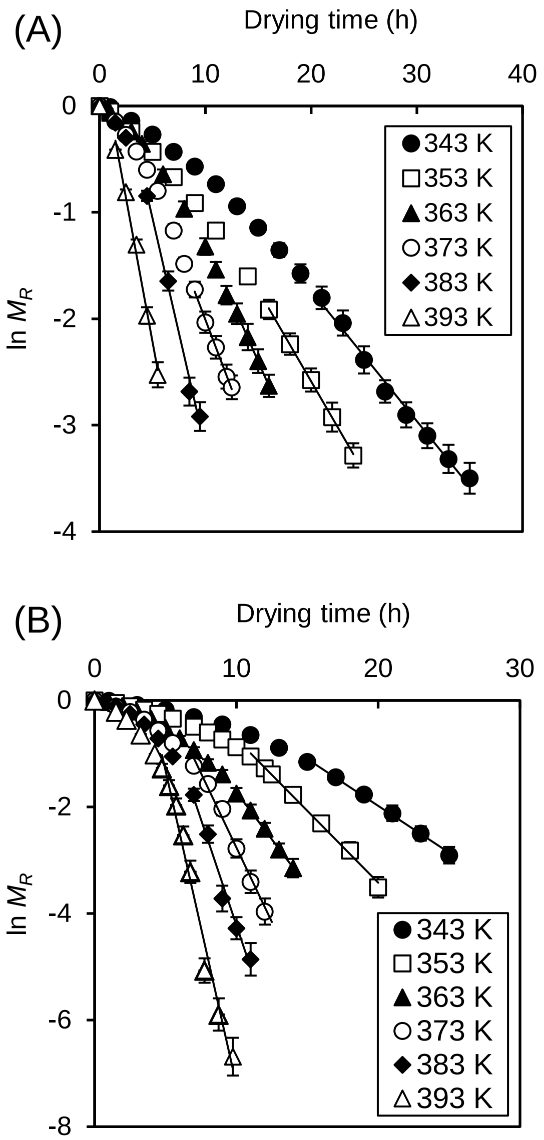

Fig. 5. Plot of ln M_R *vs* drying time, and fit of data for the falling rate period (lines). (A) WOS, (B) WOP. Sample thickness: 50 mm.

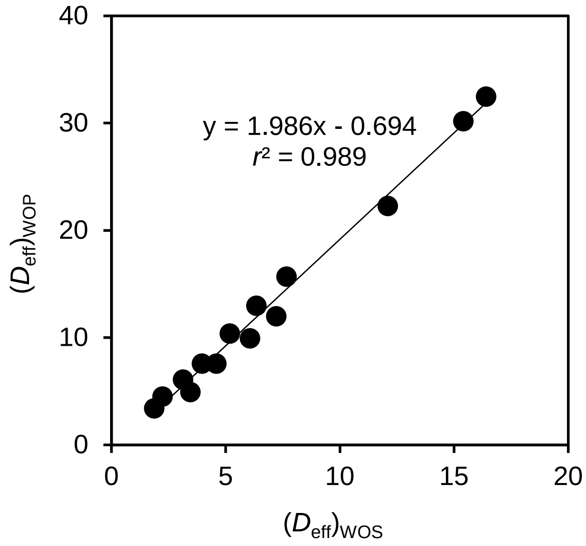

Fig. 6. Comparison between effective water diffusivities obtained with WOP and WOS.

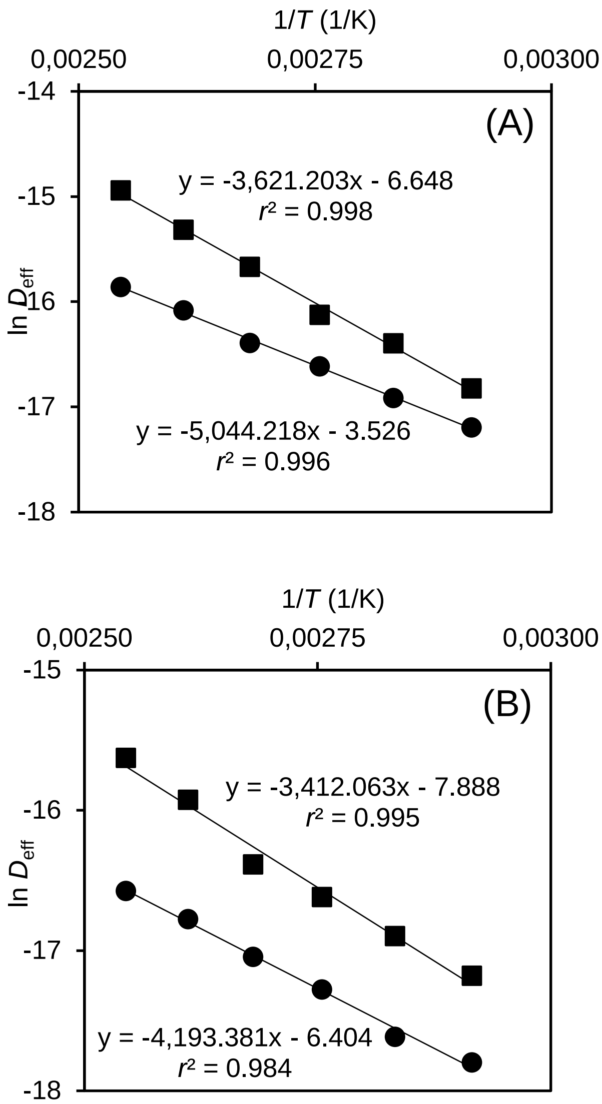

Fig 7. Relationship between effective diffusivity and temperature for the drying process of WOS (A) and WOP (B). Sample thickness: 25 mm (solid circles) and 50 mm (solid squares).

Table S1

Fit values of the mathematical models for 50 mm particle size and 70 ºC temperature

Biomass	Model name	Model constants	r^2	χ_r^2	RMSE
WOS	Lewis	*k* = 0.0768	0.992	2.29×10^{-3}	0.0467
	Page	*k* = 0.0295, *n* = 1.35	1.00	4.99×10^{-5}	0.00673
	Modified Page	*k* = 0.0740, *n* = 1.35	1.00	4.99×10^{-5}	0.00673
	Henderson and Pabis	*k* = 0.0830, *a* = 1.08	0.984	1.47×10^{-3}	0.0366
	Logarithmic	*k* = , *a* = , *c* =	0.990	1.55×10^{-3}	0.0366
	Midilli et al.	*k* = , *n* = , *a* = , *b* =	1.00	9.72×10^{-5}	0.00892
WOP	Lewis	*k* = 0.0713	0.963	9.07×10^{-3}	0.0918
	Page	*k* = 0.00953, *n* = 1.77	1.00	4.91×10^{-5}	0.00648
	Modified Page	*k* = 0.0722, *n* = 1.77	1.00	4.91×10^{-5}	0.00648
	Henderson and Pabis	*k* = 0.0806, *a* = 1.12	0.953	6.79×10^{-3}	0.0763
	Logarithmic	*k* = , *a* = , *c* =	0.953	7.41×10^{-3}	0.0763
	Midilli et al.	*k* = 0.00905, *n* = 1.79, *a* = 0.995, *b* = 0.00	1.00	5.30×10^{-5}	0.00615

WOS: Wet olive stone; WOP: Wet olive-tree pruning; χ_r^2 : Reduced chi-square; RMSE: Root mean square error.

Table S2

Fit values of the mathematical models for 50 mm particle size and 100 ºC temperature

Biomass	Model name	r^2	χ_r^2	RMSE
WOS	Lewis	0.981	3.92×10^{-3}	0.0603
	Page	1.00	7.83×10^{-5}	0.00819
	Modified Page	1.00	7.83×10^{-5}	0.00819
	Henderson and Pabis	0.977	3.01×10^{-3}	0.0508
	Logarithmic	0.977	3.28×10^{-3}	0.0508
	Midilli et al.	1.00	8.51×10^{-5}	0.00779
WOP	Lewis	0.957	1.04×10^{-2}	0.0982
	Page	0.998	2.75×10^{-4}	0.0154
	Modified Page	0.998	2.75×10^{-4}	0.0154
	Henderson and Pabis	0.947	8.41×10^{-3}	0.0849
	Logarithmic	0.947	9.17×10^{-3}	0.0849
	Midilli et al.	0.998	8.74×10^{-5}	0.00790

WOS: Wet olive stone; WOP: Wet olive-tree pruning; χ_r^2 : Reduced chi-square; RMSE: Root mean square error.

Table S3

Fit values of the mathematical models for 50 mm particle size and 120 ºC temperature

Biomass	Model name	r^2	χ_r^2	RMSE
WOS	Lewis	0.988	1.80×10^{-3}	0.0407
	Page	1.00	2.98×10^{-5}	0.00502
	Modified Page	1.00	2.98×10^{-5}	0.00502
	Henderson and Pabis	0.987	1.76×10^{-3}	0.0385
	Logarithmic	0.987	1.93×10^{-3}	0.0385
	Midilli et al.	1.00	3.60×10^{-5}	0.00499
WOP	Lewis	0.948	9.89×10^{-3}	0.0956
	Page	0.996	6.12×10^{-4}	0.0228
	Modified Page	0.996	6.12×10^{-4}	0.0228
	Henderson and Pabis	0.937	9.01×10^{-3}	0.0873
	Logarithmic	0.937	9.91×10^{-3}	0.0873
	Midilli et al.	0.996	6.62×10^{-4}	0.0214

WOS: Wet olive stone; WOP: Wet olive-tree pruning; χ_r^2 : Reduced chi-square; RMSE: Root mean square error.